Nanoscale

Accepted Manuscript

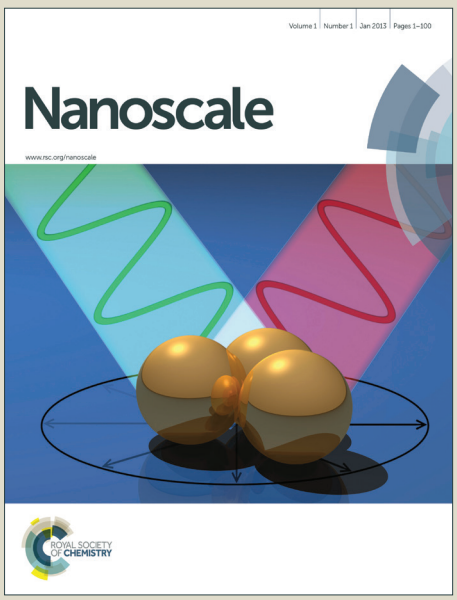

ROYAL SOCIETY OF CHEMISTRY

www.rsc.org/nanoscale

Nanoscale

Cite this: DOI: 10.1039/c0xx00000x

ARTICLE TYPE

www.rsc.org/xxxxxx

Hydrothermal-assisted Synthesis of $Na_7V_4(P_2O_7)_4(PO_4)$/C Nanorod and Its Fast Sodium Intercalation Chemistry in Aqueous Rechargeable Sodium Battery

Chao Deng,*[a] Sen Zhang*[b] and Yongxin Wu[a]

Received (in XXX, XXX) Xth XXXXXXXXX 20XX, Accepted Xth XXXXXXXXX 20XX
DOI: 10.1039/b000000x

Both high safety and low cost give aqueous rechargeable sodium-ion battery (ARSB) the opportunity for application in stationary energy storage, but the low operating potential of the existing cathode materials limits its energy density. Here, we introduce a hydrothermal-assisted strategy to prepare $Na_7V_4(P_2O_7)_4(PO_4)$/C nanorod and employs it as a novel high-property cathode material for ARSB. The hierarchical structure is directly *in-situ* carbonization from the surfactants (CTAB and oxalic acid) along with the crystallization of $Na_7V_4(P_2O_7)_4(PO_4)$. The prepared $Na_7V_4(P_2O_7)_4(PO_4)$ with well-defined 1D nanostructure and uniform particle sizes is wrapped by a thin carbon layer. For the first time, its sodium intercalation chemistry in aqueous electrolyte was investigated. Based on the reversible phase transformation and high sodium diffusion coefficient, it is demonstrated to be reliable in aqueous electrolyte with rapid ion transport capability. A pair of redox plateaus is observed in the charge and discharge curves at 0.961 and 0.944 V (vs. SCE) respectively with the capacity of 51.2 mAh·g^{-1} at 80 mA·g^{-1}. Favored by the open ion channel and 1D morphology, the composite exhibits superior high rate capability and 72% of the capacity remains at 1000 mA·g^{-1}. The results not only demonstrate a high-property cathode material for ARSB, but also are helpful for design and synthesis of mixed-polyanion electrode material with tailored architecture.

KEYWORDS: Multipolyanion material; one-dimensional nanostructure; Aqueous sodium-ion battery; sodium intercalation chemistry

Introduction

The development of solar and wind energy demands more efficient energy storage systems. Rechargeable batteries are capable of storing electricity in the form of chemical energy. Aqueous solutions have several advantages over organic solutions, for example higher ionic conductivity, lower cost and higher safety. These advantages make aqueous rechargeable batteries suitable for stationary applications[1,2]. Aqueous sodium ion batteries operating in a rocking chair manner have attracted a great deal of interest[3,4]. The natural abundance and low cost of sodium make aqueous sodium ion batteries a promising candidate for large-scale energy storage.

Cathode material plays a crucial role in determining the electrochemical performance of aqueous sodium ion batteries, but the available cathode material is rare. The first cathode material for aqueous sodium ion batteries is $Na_{0.44}MnO_2$, which shows a low reversible capacity of 45 mAh g^{-1} within a wide potential range[5]. The Prussian blue compounds with open frame structure, i.e. $Na_xM_yFe(CN)_6$ (M=Fe, Co, Ni, Cu, etc), have recently been tested as cathode materials for aqueous sodium ion batteries[6,7]; their reversible capacities are about 60 mAh g^{-1} at the current density of 1 C and their operating potentials continuously vary with the state of charge. However, the existing cathode materials are far from satisfactory, and more innovation is needed to find a high-performance cathode material for aqueous sodium ion batteries. Mixed-polyanion materials with two kinds of polyanion groups have been indentified as sodium/lithium intercalation compounds with 3D framework structure[8-13]. $Na_7V_4(P_2O_7)_4(PO_4)$ was recently reported to have two potential plateaus close to 3.88 V (vs. Na/Na$^+$) and high cycling stability over 1000 cycles[11-13]. The noticeable high voltage redox is associated with the inductive effect between vanadium and mixed phosphate polyanion groups. This superior electrochemical performance in organic electrolyte prompts us to test its electrochemical performance in aqueous electrolyte.

Tailoring materials into nanostructure is favorable to utilize their functional property. Especially, the 1D nanostructure with shorten ion diffusion distance as well as continuous electron transport pathway has been demonstrated the superiority in "rocking-chair" electrochemical system. In our previous study, the 1D architectured $Na_7V_4(P_2O_7)_4(PO_4)$ material has been synthesized by a molten-salt strategy[13]. Although the results are promising, the high-energy consuming synthetic strategy with complicated thermal treatment steps and long calcination time increase the preparation cost and limit its practical application.

Therefore, it is necessary and challenging to develop a facile and low-cost strategy for synthesizing nanostructured $Na_7V_4(P_2O_7)_4(PO_4)$.

Following this viewpoint, we design a hydrothermal-assisted strategy to prepare $Na_7V_4(P_2O_7)_4(PO_4)$/C nanorod in this study. The cetyltrimethylammonium bromide (CTAB) and oxalic acid are simultaneously used as surfactant and carbon sources to form carbon scaffolds along with the crystallization of $Na_7V_4(P_2O_7)_4(PO_4)$. It not only effectively increases the reaction efficient but also decreases the dependence on high-temperature calcination. The prepared 1D nanostructued $Na_7V_4(P_2O_7)_4(PO_4)$/C composite is employed as a cathode material for aqueous sodium ion battery. For the first time, its sodium intercalation chemistry, including phase transformation process, sodium ion diffusion mechanism and galvanostatic charge/discharge properties, in 1 M Na_2SO_4 aqueous solution is investigated.

Experimental

The starting materials are V_2O_5, Na_2CO_3, $NH_4H_2PO_4$, oxalic acid and cetyltrimethylammoniumbromide (CTAB) with molar ratio of Na: V: P: oxalic acid: CTAB=13:4:13:12:4. Stoichiometric amount of V_2O_5 and oxalic acid were dissolved in deionized water to form VOC_2O_4 solution. Then the mixed solution of Na_2CO_3, $NH_4H_2PO_4$ were mixed with the above solution, followed by slowly dropped of CTAB solution. After sufficient stirring, the above solution was transferred to a Teflon lined autoclave and kept in an oven at 180 ^oC for 60 hours. Then the product was dried and annealed at 800 ^oC for 7 hours in an argon atmosphere. After purified the intermediate product, the $Na_7V_4(P_2O_7)_4(PO_4)$/C nanorod was obtained.

Powder X-ray diffraction (XRD, Bruker D8/Germany) using Cu Kα radiation was employed to identify the crystalline phase of the material. The experiment was performed by using step mode with a fixed time of 3 s and a step size of 0.02^o. The XRD pattern was refined by using the Rietveld method. The morphology was observed with a scanning electron microscope (SEM, HITACHI S-4700) and a transmission electron microscope (TEM, JEOS-2010 PHILIPS). The carbon content was determined by an elemental analyzer (EA, Elementar Vario EL). The vanadium concentration in the aqueous electrolyte was measured by inductively coupled plasma mass spectrometry (ICP-MS, Agilent 7500CX).

Each composite electrode was made from a mixture of the active material, carbon black and polytetrafluoroethylene (PTFE) in a weight ratio of 8:1:1. The mixture was pressed into nickel foam and then dried at 80 ^oC for 12 h in air. The effective area of each electrode is about 1 cm^2. The electrochemical performance was carried out in 1 M Na_2SO_4 electrolyte under Zive workstation (for CV measurements) and LAND battery testing system (for galvanostatic charge/discharge tests).

Results and Discussion

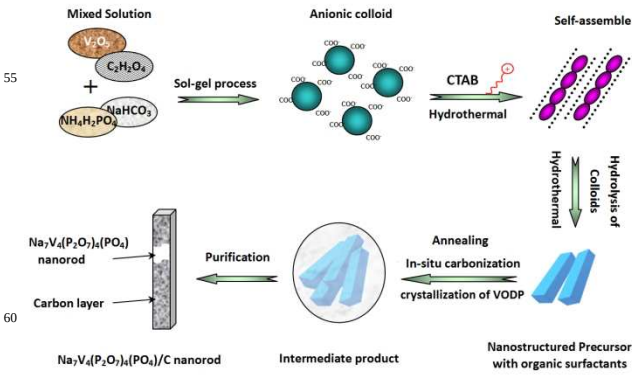

Figure 1 Schematic diagram of hydrothermal-assisted synthetic strategy for preparation of $Na_7V_4(P_2O_7)_4(PO_4)$/C nanorod.

Figure 1 illustrates the major steps and formation mechanism of hydrothermal-assisted strategy for preparation of $Na_7V_4(P_2O_7)_4(PO_4)$/C nanorod. Firstly, an anionic hydrophilic homogenous colloid is formed with mixing the VOC_2O_4 sols and the mixture solution of Na_2CO_3 and $NH_4H_2PO_4$. Then the cationic surfactant CTAB captured the anionic colloids and rearranged charge density of the solution. In the hydrothermal process, both the organic surfactants self-assemble and the colloid hydrolysis take place simultaneously, results in the formation of 1D morphology. Finally, the organic composite decomposes to *in-situ* carbon along with the $Na_7V_4(P_2O_7)_4(PO_4)$ crystallizes during calcination, and the target $Na_7V_4(P_2O_7)_4(PO_4)$/C composite was obtained after purification. The hydrothermal treatment plays an important role in controlling the surface curvature and self-assembly process, which facilitates to produce well-defined particles with lower calcination temperature and less treatment time. Therefore, the present hydrothermal-assisted strategy is proposed to be a high efficient and low lost synthetic method for preparing mixed-polyanion material with tailored architecture.

Figure 2(a) shows the XRD pattern of the $Na_7V_4(P_2O_7)_4(PO_4)$/C nanorod with the Rietveld refinement results. The calculated pattern matches well with the observed one and the values of R_p, R_{wp} and χ^2 are reasonable. The atomic parameters are displayed in Table S1 of supporting information. All the peaks can be indexed on the basis of the tetragonal structure (Space Group: $P\text{-}42_1c$) with the lattice parameters of a =14.2342 Å and c=6.3794 Å, which suggests the high purity of as-prepared samples. The morphology and detailed structure of samples are characterized by SEM and TEM observations. As displayed in Figure 2(b), the precursor is composed of bundles of nanorods, and all of the nanorods aligned along the same direction. The element mapping images (Figure 3c) certify the existence and uniform distribution of C, V, P elements. The results demonstrate that the precursor is composed of organic surfactant and hydrolyzed colloids. After calcination, the 1D nanostructure is preserved. As observed in Figure 3(d) and (e), the final product has uniform particles with the diameter of 150~250 nm and the length of 1.5~3μm. HRTEM image and the corresponding SEAD pattern (Figure 1f) demonstrate the single

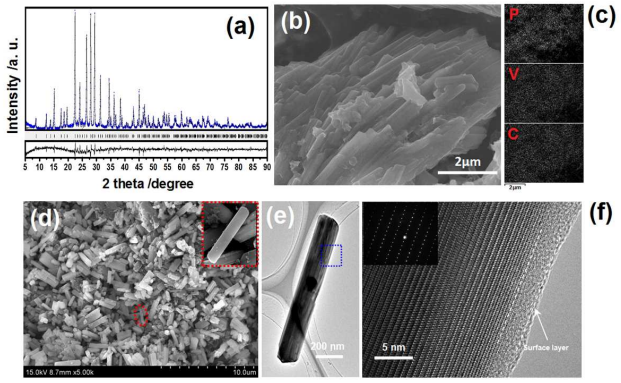

Figure 2 (a) XRD of the $Na_7V_4(P_2O_7)_4(PO_4)$/C nanorod (R_p=11.07%, R_{wp}=13.70%, χ^2=2.03); (b) SEM image and (c) elemental mapping images of the precursor; (d) SEM image of the $Na_7V_4(P_2O_7)_4(PO_4)$/C nanorod. The inset is the enlarged image of a single nanorod illustrated in red circle of d; (e) TEM image, (f) HRTEM image and SAED pattern of a single nanorod.

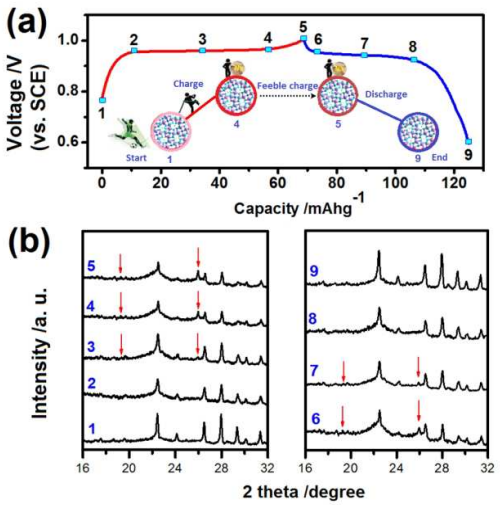

Figure 3 (a) The initial charge/discharge curves in the voltage range of 0.5~1.006 V (vs. SCE) and (b) corresponding *ex-situ* XRD patterns obtained at denoted points highlighted in (a). The schematic diagram for the charge/discharge process is illustrated in inset of a.

crystal nature of the nanorod. The results demonstrate that uniform particle sizes and well-defined 1D nanostructure can be obtained for $Na_7V_4(P_2O_7)_4(PO_4)$ by present strategy. A carbon surface layer with the thickness of 2~3 nm is observed on the surface of the nanorod. Schematically speaking (Figure 1), the inner $Na_7V_4(P_2O_7)_4(PO_4)$ nanorod are encased in the outer carbon layer. This morphology is favorable to both sodium-ion diffusion and electron conduction.

In order to get deep insight into the sodium intercalation mechanism in aqueous electrolyte, the *ex-situ* XRD measurements were carried out at different charge/discharge stages. At each point, half an hour was hold before the measurement. The first galvanostatic charge/discharge curves of the $Na_7V_4(P_2O_7)_4(PO_4)$/C nanorod in 1 M Na_2SO_4 aqueous solution are shown in Figure 3(a). A pair of well-defined redox plateaus is observed at 0.961/0.944 V in the charge/discharge curve under the current density of 40 $mA \cdot g^{-1}$, corresponding to the sodium extraction/insertion into/from the $Na_7V_4(P_2O_7)_4(PO_4)$/C nanorod. The sodium de/intercalation process is revealed by *ex-situ* XRD measurements at various charge/discharge states highlighted in Figure 3(a). The *ex-situ* XRD patterns are shown in Figure 3(b). The XRD pattern measured at Point 2 has no extra peak in comparison with that at Point 1, but the diffraction peaks weakened and widened. This indicates that the original crystal structure isn't altered by initial sodium deintercalation. Two additional peaks can be observed at 19.26° and 25.96° in the XRD pattern measured at Point 3, which indicates the formation of a new phase. The additional peaks manifest themselves upon further charging, thus the new phase accumulates and the original phase dwindles away until the end of charge (Point 4 and 5). This phase transition process is fully reversible upon discharging (Point 6, 7, 8 and 9), and the original material is recovered at the end of discharge (Point 9). The phase transition is similar to that observed in organic electrolyte[11,12], and the only difference is whether the material is fully utilized. The $Na_7V_4(P_2O_7)_4(PO_4)$/C nanorod is not fully utilized in aqueous solution because a portion of the original phase still exists at the end of charge (Point 5). In other words, the phase transformation is incomplete in aqueous electrolyte, which is partial associated with the lower cut-off voltage in aqueous system. ICP results indicate that the ratio of sodium and vanadium for the fully charged and discharge states are about 1.06 and 1.69. Thus about 2.52 sodium atoms per formula are exchanged during (de)intercalation process, which is coincided with the *ex-situ* XRD and electrochemical results. Based on above results, the incomplete phase transformation lowered the attainable capacity in aqueous electrolyte which is only two thirds of that in organic electrolyte. Nonetheless, the reversible phase transition during charge-discharge cycling makes the $Na_7V_4(P_2O_7)_4(PO_4)$/C nanorod a promising cathode candidate for aqueous sodium-ion battery.

The CV curves at various scan rates were recorded to study the sodium intercalation behavior of $Na_7V_4(P_2O_7)_4(PO_4)$/C nanorod (Figure 4a). A pair of redox peaks is observed in each curve, and the peak current increases with increasing scan rate. Moreover, there is a linear relationship between the anodic/cathodic peak current and the square root of scan rate (Figure 4b,c), indicating that the controlling step of the sodium intercalation process is sodium-ion diffusion. Therefore, the diffusion coefficient of sodium-ion (D_{Na}) can be calculated on the basis of the Randles-Sevcik equation[14],

$$i_p = 0.4463\left(\frac{F}{RT}\right)^{1/2} n^{3/2} A D_{Na}^{1/2} C^* v^{1/2} \quad (1)$$

Where i_p, n, A, C^* and v are the peak current, number of exchanged electrons, surface area, sodium concentration and sweep rate, respectively. The average diffusion coefficient (D_{Na}) is calculated to be 3.9×10^{-11} $cm^2 \cdot s^{-1}$, which is higher than those of other sodium-intercalation materials (10^{-12}~10^{-14} $cm^2 \cdot s^{-1}$)[3,15-17]. Higher diffusion coefficient is clearly an indicator of faster sodium-ion transport within the $Na_7V_4(P_2O_7)_4(PO_4)$/C nanorod.

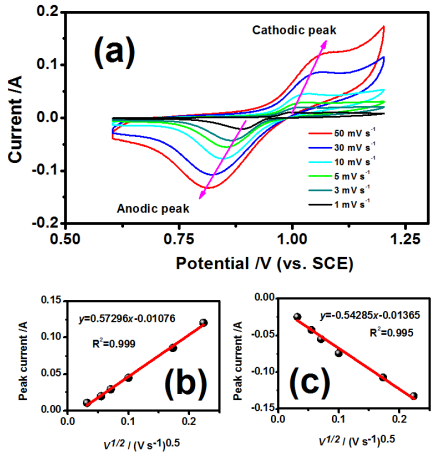

Figure 4 (a) CV curves at various scan rate from 1 to 50 mV·s^{-1}. The relationship between the cathodic (b) and anodic (c) peak currents and the square root of the potential sweep rates.

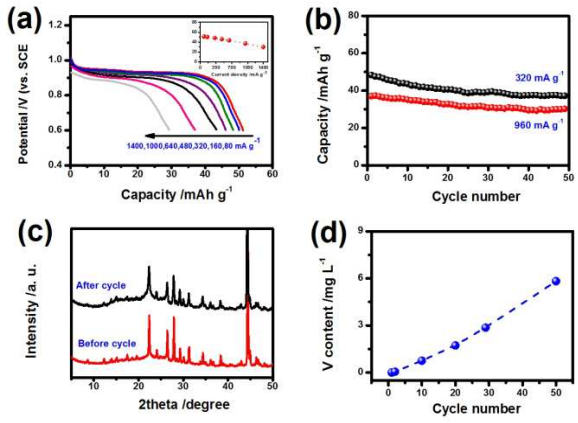

Figure 5 (a) discharge curves obtained at various current densities. The obtained capacities are compared in the inset of a; (b) cycling property at 320 and 1000 mAh·g^{-1}; (c) *ex-situ* XRD patterns before and after cycles; (d) the changes of vanadium content in the aqueous electrolyte during cycling.

The electrochemical performance of the $Na_7V_4(P_2O_7)_4(PO_4)$/C nanorod is shown in Figure 5. The high-rate capability is fairly favorable. A significant increase of current density from 80 to 320 mA·g^{-1} results in a slight decrease of discharge capacity from 51.2 to 48.3 mAh·g^{-1} (Figure 5a). The discharge capacity of 37.0 mAh·g^{-1} is still delivered even if the current density is as high as 1000 mA·g^{-1}, corresponding to 72% of the discharge capacity obtained at the current density of 80 mA·g^{-1}. The desirable high-rate capability can be attributed to the fast sodium-ion transport which is favored by the structural and morphological characteristics. The 3D open framework structure of $Na_7V_4(P_2O_7)_4(PO_4)$ provides well-defined channels for sodium-ion exaction/insertion; the carbon-coated nanorod morphology provides short pathway for sodium-ion diffusion, carbon layer for electron conduction and large area for charge transfer reaction. The cycling performance is evaluated at two current densities, i.e. 320 and 1000 mA·g^{-1} (Figure 5b). After fifty cycles, the retention ratios of the first discharge capacities are 77% and 82%, respectively. The *ex-situ* XRD pattern of the cycled electrode was collected in Figure 5(c). The XRD pattern of the cycled electrode has no extra peaks in comparison with the XRD pattern of the original electrode, but the diffraction peaks weaken and broaden upon cycling. Vanadium dissolution is revealed by monitoring the vanadium concentration in the aqueous electrolyte (Figure 5d), which is the main reason for capacity fading. The high operating potential and superior high-rate capability of the $Na_7V_4(P_2O_7)_4(PO_4)$/C nanorod is desirable for advanced aqueous rechargeable sodium-ion battery.

Conclusions

In summary, we put forward a hydrothermal-assisted synthetic strategy for preparing $Na_7V_4(P_2O_7)_4(PO_4)$/C nanorod and introduce it as a new cathode material for aqueous sodium ion battery. The approach is high-efficient and low-cost with simultaneously *in-situ* carbonization of surfactants (CTAB and oxalic acid) and crystallization of the nanorod. The prepared well-defined $Na_7V_4(P_2O_7)_4(PO_4)$ nanorod are wrapped by a thin carbon layer, and its sodium intercalation chemistry in aqueous electrolyte was investigated for the first time. The reversible phase transformation is revealed by *ex-situ* XRD patterns measured during the first galvanostatic charge-discharge cycle. The desirable structural and morphological characteristics enable the $Na_7V_4(P_2O_7)_4(PO_4)$ nanorod to have high sodium-ion diffusion coefficient (D_{Na}) and superior high-rate capability. The favorable sodium intercalation chemistry in 1 M Na_2SO_4 aqueous electrolyte makes the $Na_7V_4(P_2O_7)_4(PO_4)$ nanorod a feasible cathode material for advanced aqueous rechargeable sodium-ion battery. This fundamental work not only introduces a novel high-property cathode material for ARSB, but also provides guidelines for design and synthesizes mixed polyanion material with tailored architecture.

Acknowledgements

This work is supported by the National Natural Science Foundation of China (No. 21001036, 50902041), Program for New Century Excellent Talents in Heilongjiang Provincial University (1253-NCET-012) and Natural Science Foundation of Heilongjiang Province (No. QC2013C008).

Notes and references

[a] *Key Laboratory for Photonic and Electronic Bandgap Materials, Ministry of Education; College of Chemistry and Chemical Engineering, Harbin Normal University, Harbin, 150025, Heilongjiang, China; E-Mail: chaodenghsd@sina.com*

[b] *Key Laboratory of Superlight Material and Surface Technology, Ministry of Education, College of Material Science and Chemical Engineering, Harbin Engineering University, Harbin 150001, Heilongjiang, China; E-Mail: senzhang@hrbeu.edu.cn*

1 M. Pasta, C. D. Wessells, R. A. Huggins, Y. Cui. *Nat. Commun.* 2012, ***3***, 1149-1153.

2 W. Li, J. R. Dahn, D. S. Wainwright, *Science* 1994, ***264***, 1115-1118.

3 C. Deng, S. Zhang, Z. Dong, Y. Shang, *Nano Energy* 2014, ***3***, 14-19.

4 Z. Li, D. Young, K. Xiang, W. C. Caeter, Y. M. Chiang,. *Adv. Energy Mater*. 2013, ***3***, 290-294.

5 J. F. Whitacre, A. Tevar, S. Sharma, *Electrochem. Commun.* 2010, ***12***, 463-466.

6 X. Y. Wu, Y. L. Cao,X. P. Ai, J. F. Qian, H. X. Yang, *Electrochem. Commun.* 2013, ***31***, 145-148.

7 X. Y. Wu, M. Y. Sun, Y. F. Shen, J. F. Qian, Y. L. Cao,X. P. Ai, H. Yan, *ChemSusChem* 2014, ***7***, 407-411.

8 H. Kim, I. Park, D. H. Seo, S. Lee, S. W. Kim, W. J. Kwon, Y. U. Park, C. S. Kim, S. Jeon, K. Kang, *J. Am. Chem. Soc*. 2012, ***134***, 10369-10372.

9 H. Kim, I. Park, S. Lee, H. Kim, K. Y. Park, Y. U. Park, H. Kim, J. Kim, H. D. Lim, W. S. Yoon, K.Kang, *Chem. Mater*. 2013, ***25,*** 3614-3622.

10 1Q. Kuang, J. T. Xu, Y. M. Zhao, X. L. Chen, L. Q. Chen, *Electrochim. Acta* 2011, ***56***, 2201-2205.

11 S. Y. Lim, H. Kim, J. Chung, J. H. Lee, B. G. Kim, J. J. Choi, K. Y. Chung,, W. Cho, S. J. Kim, W. A. Goddard, Y. S. Jung, J. W. Choi, *PNAS* 2014, ***111***, 599-604.

12 S. Y. Lim, J. W. Choi, *224th ECS Meeting* 2013, *369*

13 C. Deng, S. Zhang, *ACS Appl. Mater. Interfaces* 2014, **6,** 9111-9117.

14 A. Bard, L. R. Faulkner, *Electrochemical Methods*, *2nd ed*. Wiley press: New York, 2001.

15 Zhao, M. S.; Huang, G. L.; Zhang, W. G.; Zhang, H. Y.; Song, X. P. *Energy Fuels* **2013**, *27*, 1162-1167.

16 M. S. Wu, P. C. Chiang, *Electrochem. Commun.* 2006, ***8***, 383-388.

17 N. Bockenfeld, A. Balducci, *J. Solid State Electrochem.* 2014, ***18***, 959-964.